

## **NUMERICAL SIMULATION OF THE ROTATING CAGE PROBLEM**

**Prabhu Ramachandran**

Department of Aerospace Engineering  
IIT Bombay  
Mumbai  
INDIA 400076  
Email: prabhu@aero.iitb.ac.in

### **ABSTRACT**

The rotating cage apparatus is used in the oil industry as a simple and effective test for corrosion. The apparatus generates a large amount of flow induced corrosion and is used by researchers to design effective corrosion inhibitors. While the apparatus is used frequently, the fluid mechanics of the problem is not well understood. Importantly, there is no correct model for the shear stress profile. In this paper we study the unsteady fluid dynamics of the rotating cage problem. We consider an equivalent, idealized, two-dimensional problem for a Newtonian fluid and perform high resolution simulations of the rotating cage using a vortex method. The vortex method is a particle method that is well suited to complex geometries, unsteady flow and capable of high resolution. We present initial results of various simulations performed at different Reynolds numbers. The shear stress is computed and compared with currently used models.

### **INTRODUCTION**

Oil and gas operations involve the transport of oil and gas at high pressure and flowing at significant speeds. Oil and gas pipelines transport a large amount of material and are usually of very large lengths. The flowing oil and gas can corrode the pipelines. Frequent replacement of these pipelines is expensive in terms of down time and material costs. Oil companies therefore use corrosion inhibitors to reduce the amount of corrosion. These corrosion inhibitors are usually proprietary chemicals that are added in small quantities. They significantly reduce the amount of corrosion due to the flow.

If one is to create effective corrosion inhibitors, it is important to be able to test the effectiveness of the inhibitor in the laboratory using a simple experiment in a repeatable fashion. There are many experimental techniques that are well suited to producing high amounts of flow induced localized corrosion (FLIC). The various experimental techniques to do this are critically reviewed in Schmitt and Bakalli [1].

The rotating cage is one such apparatus that is recommended by several researchers as an appropriate test for corrosion inhibitor performance under severe conditions. The apparatus consists of a collection of flat blades (called coupons) arranged along the circumference of a cylinder. This cage of blades is placed inside a cylinder filled with a viscous fluid. Fig. 1 is a sketch of a rotating cage apparatus. The cage is rotated at high speed for several hours. In [2] the test is run for 18 hours and in [3] for 120 hours. The coupons are weighed before the experiment is started. At the end of the experiment they are cleaned and weighed again. The difference in weight divided by the time taken provides an average corrosion rate. The coupons are also inspected visually to provide an idea of the kind of corrosion that occurs.

The apparatus can also be used under high pressure and temperature [2]. This approach is commonly referred to as the "high speed autoclave test" (HSAT). The rotating cage has been successfully used in practice to develop a large number of corrosion inhibitors [4, 2, 3]. The important advantages of the rotating cage apparatus are that it is relatively easy and inexpensive to setup and use, it is easy to reproduce high pressure and high temperature conditions, the coupons experience a very large shear stress and therefore experience severe flow conditions. Corrosion in-

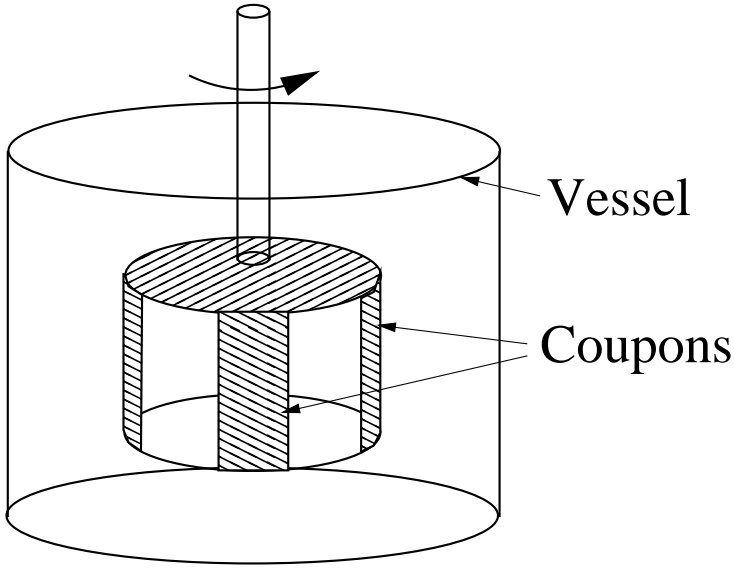


Figure 1. Sketch of a rotating cage apparatus.

hibitors that perform well in this apparatus always appear to perform well in the field.

The fluid mechanics of various other corrosion inhibitor apparatuses like pipe flow, rotating cylinder electrode and jet impingement apparatus are well established. However, the rotating cage problem is not as well studied. As explained by Schmitt and Bakalli [1], it is sometimes possible to relate the corrosion rate to the shear stress experienced by the coupons using the equation,

$$W = a\tau^b \quad (1)$$

where  $W$  is the corrosion rate,  $\tau$  the shear stress and  $a, b$  are constants depending on the flow, fluid and conditions.

If a rotating cage is spinning with angular velocity  $\Omega$  and has a radius  $R_c$ , then the Reynolds number of the flow is defined as,

$$Re = \frac{\Omega R_c^2}{\nu} \quad (2)$$

where  $\nu$  is the kinematic viscosity of the fluid. According to Schmitt and Bakalli [1] the shear stress on the coupon may be given by,

$$\tau = 0.0791 Re^{-0.3} \rho R_c^2 \Omega^{2.3} \quad (3)$$

Equation (3) is essentially based on the shear stress experienced by a rotating cylinder. One would expect that the flow

experienced by a coupon in a rotating cage would be similar to that of the turbulent flow past a flat plate rather than the flow over a rotating cylinder. This was even suggested by Dougherty et al. [4] in their work. They suggest that the correct shear stress profile would be that of a flat plate and use the following equation,

$$\tau = \frac{3}{9.28} \sqrt{\frac{\rho \mu \Omega R_c}{x}}, \quad (4)$$

where  $\mu$  is the dynamic viscosity of the fluid and  $x$  is the distance from the leading edge of the coupon. This equation explains the severe amount of corrosion that the authors in [4, 3] experimentally observe at the leading edges of the coupons. However, it appears that other researchers [1] continue to use the shear stress expression arising from the flow over a rotating cylinder.

The rotating cage problem does not appear to have been simulated numerically in the literature. As an initial attempt in this direction, we numerically simulate the unsteady flow inside a rotating cage in this paper. We consider an idealized two-dimensional problem of four flat plates (having zero thickness) that are spinning inside a circular cylinder. The fluid is assumed to be incompressible, single-phase and Newtonian.

We use a vortex method [5, 6, 7, 8] for the numerical simulation. The vortex method is a particle based method and is grid free. The vorticity field is discretized into particles that carry the vorticity. The evolution of the vorticity field is calculated by tracking the vortex particles in a Lagrangian fashion. The method is designed for unsteady flows. It is self-adaptive in that computational particles are only used in areas where they are necessary. Since there is no fixed grid, numerical dissipation is minimized. The method is well suited for high-resolution and can handle complex geometries and moving bodies.

In this work, we use the vortex method to study the shear stress profile along the coupon's surface when it is subjected to the flow inside a rotating cage.

It is to be noted that the fluid flow in the rotating cage is inherently three dimensional. The two-dimensional treatment in this work is a rather gross simplification. However, it does serve to help understand the complexities involved in the two dimensional case. The present results also allow for an interesting comparison between more realistic three dimensional simulations. The three dimensional simulation is a lot harder to perform and it is important that such computations be performed in the future in order to obtain a better understanding of the problem.

In the subsequent sections we provide a brief overview of the governing equations, the numerical scheme, algorithms and parameters used by the vortex method. This is followed by the results of the simulation. We simulate the problem at various Reynolds numbers and compare the shear stress profile that we compute. We also show the vorticity field generated by the sim-

ulation for the different cases considered.

## GOVERNING EQUATIONS

The equations we solve in the present work are the Navier-Stokes (NS) equations in the vorticity-velocity form. The vorticity  $\vec{\omega}$ , is the curl of the velocity field,  $\vec{\omega} = \text{curl } \vec{V}$ . For a two-dimensional flow, only the component of the vorticity out of the plane needs to be considered. Thus,  $\omega = \hat{k} \cdot \text{curl } \vec{V}$ , where  $\hat{k}$  is the unit vector out of the plane of the flow. If the curl of the NS equations in primitive variables is taken we obtain the vorticity-velocity formulation.

If the fluid is incompressible, the fluid flow may be completely represented by the vorticity alone. For the flow past a body  $B$ , in two-dimensions, the governing differential equations along with the boundary conditions are given by,

$$\frac{\partial \omega}{\partial t} + \vec{V} \cdot \text{grad } \omega = \nu \nabla^2 \omega, \quad (5a)$$

$$\text{div } \vec{V} = 0, \quad (5b)$$

$$\omega(\vec{r}, 0) = \omega_0(\vec{r}), \quad (5c)$$

$$\vec{V}(\vec{r}, t) \cdot \hat{e}_n = \vec{V}_B \cdot \hat{e}_n \quad \text{on boundary of } B, \quad (5d)$$

$$\vec{V}(\vec{r}, t) \cdot \hat{e}_s = \vec{V}_B \cdot \hat{e}_s \quad \text{on boundary of } B, \quad (5e)$$

where  $\nu$  is the kinematic viscosity,  $\hat{e}_n$  and  $\hat{e}_s$  are the normal and tangential unit vectors on the boundary of  $B$ .

In the present work we employ the Random Vortex Method (RVM) [5, 9, 10, 8]. The RVM uses operator splitting to solve equation (5) in two steps during each time step. The equations are called the advection and diffusion equations and are given by,

$$\frac{D\omega}{Dt} = 0, \quad (\text{Advection}) \quad (6a)$$

$$\frac{\partial \omega}{\partial t} = \nu \nabla^2 \omega. \quad (\text{Diffusion}) \quad (6b)$$

This approach enables for a Lagrangian method of solution. In the vortex method, the vorticity field  $\omega$  is discretized into particles carrying it. These particles are tracked as per the equations (6). The advection equation implies that any existing vorticity is convected along with the flow. The diffusion equation simulates the viscous diffusion of the vorticity.

## Vortex blobs and sheets

In the present work we employ two different types of particles to discretize the vorticity. Vortex sheets [9, 11] are used in a thin region around the body called the *numerical layer*. A vortex

sheet is essentially a flat element having a vorticity strength (circulation per unit length),  $\gamma$ , and a length,  $\lambda$ . Outside the numerical layer the vorticity field is discretized in the form of vortex blobs. Vortex blobs are spherically symmetric and have a functional variation of vorticity in them given by  $f_\delta$ , a circulation of  $\Gamma$  and core-radius,  $\delta$ , that determines the extent of the blob.

In the numerical layer, the boundary layer equations are assumed valid. The velocity field induced by a vortex sheet is needed for the advection step (equation (6a)). If the strength of a sheet is  $\gamma$ , its length is  $\lambda$  and if the sheet is parallel to the  $x$ -axis and starting at the origin then its velocity at a point  $(x, y)$  is given as

$$\vec{V}(x, y) = (u, v) = \begin{cases} (-\gamma, 0) & 0 < x < \lambda; y < 0, \\ (0, 0) & \text{otherwise.} \end{cases} \quad (7)$$

When a sheet leaves the numerical layer it is converted into a vortex blob such that its circulation  $\Gamma = \gamma\lambda$  and its core radius  $\delta = \lambda/\pi$ . More details on vortex sheets may be had from [9, 11, 12, 8].

Outside the numerical layer vortex blobs are used to discretize the vorticity field. The vorticity in this region is discretized as,

$$\omega(\vec{x}) = \sum_{j=0}^N f_\delta(\vec{x} - \vec{x}_j) \Gamma_j. \quad (8)$$

where  $\vec{x}_j$ ,  $\Gamma_j$  are the position and circulation respectively of each blob.  $\delta$  is as mentioned earlier the core-radius. The order of the accuracy of the vortex blob method depends on the nature of the smoothing function,  $f_\delta$ . In the present work we use Chorin's blob [5], which is a second-order blob (i.e. the error involved in the discretization is of the form  $\delta^2$ ).

For a vorticity field,  $\omega(\vec{x}, t)$ , the corresponding velocity field,  $\vec{V}_\omega$  can be obtained as,

$$\vec{V}_\omega(\vec{x}, t) = \sum_{j=0}^N K_\delta(\vec{x} - \vec{x}_j) \Gamma_j, \quad (9)$$

where  $K_\delta$  is the desingularized velocity kernel. The velocity kernel may itself be related to  $f_\delta$  and the Cauchy velocity kernel (the velocity due to a point vortex) as,

$$K_\delta = K(x, y) * f_\delta = \frac{(-y, x)}{2\pi r^2} * f_\delta, \quad (10)$$

where  $*$  denotes convolution and  $r^2 = x^2 + y^2$ . Thus, the velocity field corresponding to a given vorticity field can be obtained depending on the nature of the function  $f_\delta$ .

## Boundary conditions

The far field boundary condition is automatically satisfied since the influence of the vortex particles is by construction zero at infinity. There are two boundary conditions that are to be enforced. These are the no-penetration boundary condition on the surface of the solid body (equation (5d)) and the no-slip boundary condition (equation (5e)).

Given the discretized vorticity field in the form of vortex blobs and sheets one can obtain the velocity field,  $\vec{V}_\omega$  as detailed in the previous sub section. In general this  $\vec{V}_\omega$  will not satisfy the no-penetration boundary condition on the boundary of the body  $B$ . This may be satisfied by adding a suitable potential velocity field. Since the curl of the potential field is zero, it does not affect the vorticity field.

The no-slip boundary condition is satisfied at each time step by releasing vorticity in the form of vortex sheets on the surface of the body.

## Solution of advection and diffusion equations

Given a velocity field that satisfies the no-penetration and slip boundary conditions, the advection equation may be solved by integrating a system of ODEs that govern the position of the vortices.

The diffusion equation (6b) is simulated using the method of random walks [5]. In this method the vortex particles are made to undergo independent random walks with their displacement drawn from a Gaussian distribution having zero mean and variance  $2\nu\Delta t$ , where  $\Delta t$  is the timestep.

## NUMERICAL METHOD

The numerical implementation of the vortex method involves several algorithms. As seen in the previous section, the two main steps involved are those of advection and diffusion. During the advection of the particles the no-penetration and no-slip boundary conditions are to be satisfied.

The advection equation (6a) is solved by finding the velocity field due to the vorticity and the no-slip boundary condition. This velocity field is used to integrate a system of ODEs describing the position of the particles. The numerical integration is performed using a second order Runge-Kutta scheme. The efficient computation of the velocity field due to the vortex particles is an issue. If there are  $N$  vortex blobs then a naive computation of the velocity of these  $N$  particles would require an  $O(N^2)$  number of computations. This is prohibitively expensive since  $N$  can be extremely large. This computation is therefore accelerated to an  $O(N)$  process by using an Adaptive Fast Multipole Method (AFMM) [13].

In order to satisfy the no-penetration boundary condition an accelerated higher order vortex panel method [14, 15] is used.

The no slip boundary condition is satisfied by releasing vortex sheets on the surface of the body. In order to do this, the slip velocity over a collection of control points placed on the surface of the body is computed. Vortex sheets are released on the surface of the body such that this slip velocity is nullified. Care is taken to limit the strength of the sheets by  $\gamma_{max}$ . Thus, if  $|u_s|$  is the slip velocity at a particular location then  $\lceil |u_s|/\gamma_{max} \rceil$  sheets of strength  $\gamma_{max}$  are released, where  $\lceil x \rceil$  is the largest integer less than  $x$ . The remaining amount of slip is satisfied by adding a single sheet of suitable strength less than  $\gamma_{max}$ . Thus, all vortex particles have their circulations bounded by  $\gamma_{max}\lambda$ .

As discussed in section , diffusion is solved by the method of random walks. The random numbers are generated by using a pseudo random number generator.

As the particles move about due to advection and diffusion, it is possible for them to intersect the boundaries. This especially true for the diffusion step. These particles are specularly reflected using an efficient algorithm [16].

In the RVM it is often found that particles of opposite sign are very close to each other. If two particles of opposite sign and same magnitude of circulation are found within a radius of  $R_a\lambda$ , then they are annihilated. Similarly if there are two particles of the same sign but whose strengths are together less than  $\gamma_{max}$ , then they are merged such that the first moment of the vorticity is preserved. This has been found [8] to significantly reduces the number of particles and also improves the accuracy of the simulations.

More details on the method and the various algorithms are available in [8].

## Numerical parameters

There are various parameters involved in the numerical implementation of the RVM. These may be inter-related in order to produce a few crucial and physically relevant parameters.

If the height of the numerical layer is  $h_{num}$ , then in order to ensure that vortex blobs do not penetrate the solid surfaces we must ensure that the core radius  $\delta \leq h_{num}$ .

Let the length of the solid surface be  $L$ , then if  $N$  sheets are released from the surface, their lengths are  $\lambda = L/N$ , thus  $\delta = L/(N\pi)$ . We therefore can say that  $L/(N\pi) \leq h_{num}$ . Now,  $h_{num}$  may itself be related to an approximate boundary layer height as,

$$h_{num} = \frac{kL}{\sqrt{Re}}, \quad (11)$$

where  $k$  is a length scale determining a fraction of this crude boundary layer height. Thus we have that

$$N \geq \frac{\sqrt{Re}}{\pi k} \quad (12)$$

Once  $N$  is known, the size of the sheet and blobs are determined.  $k$  is clearly a length scale. One can also choose a time scale for the time integration by limiting the distance a vortex sheet will travel in one time step by,

$$\Delta t = \frac{CL}{UN}, \quad (13)$$

where  $U$  is an approximate maximum velocity. Thus  $C$  is a time scale.

In addition to these two parameters we also have the parameter  $\gamma_{max}$  and the radius of annihilation and merging,  $R_a$ . The lower the value of  $\gamma_{max}$ , the better, however it is a good idea to choose it such that the cell Reynolds number  $Re_h$ , is  $O(1)$ . The cell Reynolds number is given as,

$$Re_h = \frac{\gamma_{max}\lambda}{\nu} \quad (14)$$

Finally, the parameter  $R_a, R_m$  for the annihilation and merging of particles is chosen to be 0.5. If the distance between two particles is less than  $R_a\lambda$ , then they are considered for merging and annihilation.

Thus we have 4 parameters.  $k, C$  are length and time scale parameters.  $\gamma_{max}$  and  $k$  (through  $\lambda$ ) allows us to limit the cell Reynolds number. This ensures that all relevant physical scales are resolved. Finally  $R_a$  and  $R_m$  are numerical parameters to help reduce the number of particles.

## RESULTS AND DISCUSSION

### Simulated problem

In the present work we simulate the rotating cage problem numerically using the vortex method. We solve an idealized 2D problem and use an incompressible, single-phase, Newtonian fluid. Fig. 2 sketches the geometry considered and the various quantities involved. Four coupons are used. The coupons are flat plates having zero thickness.

For the rotating cage problem the Reynolds number is usually given by equation (2),

$$Re = \frac{\Omega R_c^2}{\nu}$$

In order to make meaningful simulations we first get a rough idea of the values of  $Re$  used by the community. The fluid typically used is water (actually brine is used). We assume a temperature of 298.16 K (25°C). The dynamic viscosity,  $\nu$ , of water at this temperature may be taken to be  $0.89 \times 10^{-6} m^2/s$ .

We assume typical values of various lengths to be  $R_c = 1.25, L = 1, R = 2$  inches.  $\Omega$  is typically in the range 50 to 2000

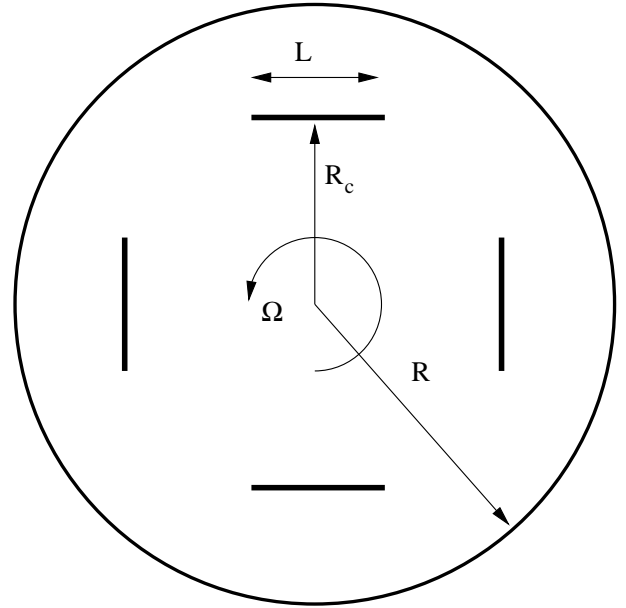


Figure 2. Simulated problem and quantities involved.

RPM. This gives us a Reynolds number range of around 5000 to 250000. This is a very large range. In this paper we restrict our attention to values between 5000 and 50000.

At this point it is important to define non-dimensional quantities relevant to the simulation. We define the Reynolds number of flow over the coupon as,

$$Re_c = \frac{\Omega R_c L}{\nu}. \quad (15)$$

This is done because the flow over the coupon is effectively that of the flow past a flat plate for which the Reynolds number is defined as above. We also define the following non-dimensional numbers,

$$l_c = \frac{L}{R_c}, \quad (16)$$

$$l_v = \frac{R}{R_c}, \quad (17)$$

$$T = \frac{\Omega t}{2\pi}. \quad (18)$$

$T$  is clearly a non-dimensional time that indicates the number of rotations a coupon makes. The other two are useful length ratios.

### Grid independence study

We start by performing a simple grid independence study. In the present work we are interested mainly in the shear stress

profile along the plate. Thus we choose parameters in order to ensure that these are captured correctly.

We consider  $Re = 20000$  for the purposes of the study. We assume that  $R_c = 0.05\text{m}$ ,  $l_c = 0.5$  and  $l_v = 1.6$ . To attain  $Re = 20000$ , from equation (2), we have  $\Omega \approx 7.12\text{rad/s}$  (68rpm). We also clearly see that  $Re_c = 10000$ . The various numerical parameters are chosen as discussed in section . We note that the Reynolds number that is to be considered is  $Re_c$  when choosing these parameters. This is because the fluid flow over the coupons is what generates the vorticity.

The parameters  $k$  and  $C$  must be chosen carefully in order to simulate the physics correctly. We hold all other parameters fixed and vary either  $C$  or  $k$  to get the optimal parameters. Table 1 shows the various values considered for this study.  $N_{sheet}$  is the number of control points on which the no-slip boundary condition is satisfied on one side of a coupon.

Case	$k$	$C$	$N_{sheet}$	$\Delta t$	$\gamma_{max}$	$Re_h$
1a	0.2	22.8	160	0.01	0.025	4.4
1b	0.2	11.4	160	0.005	0.025	4.4
1c	0.2	5.7	160	0.0025	0.025	4.4
2a	0.4	11.4	80	0.01	0.025	8.8
2b	0.4	5.7	80	0.005	0.025	8.8
3	0.8	5.7	40	0.01	0.025	17.6
4	1.6	2.85	20	0.01	0.025	35.2

Table 1. Parameters varied to obtain optimal values.  $N_{sheet}$  is the number of control points on which the no-slip boundary condition is satisfied on one side of a coupon.  $Re_h$  is the cell Reynolds number.

In order to pick the best of these parameters we consider the shear stress profile on the outer surface of the coupon. For all cases in this grid independence study except case 1c we simulate the problem till  $T = 5.67$ , i.e. each coupon has performed more than five and a half rotations. Case 1c is simulated only till  $T = 1.7$ . This is because it takes twice as long as case 1b to execute.

We first plot the shear stress versus the length of the coupon along the outer surface. We plot the average of the shear stress over all the coupons at several instants of time. The flow is highly unsteady (as we will see later) and therefore it makes little sense to consider instantaneous shear stresses. We therefore perform a time average of the data over several timesteps. Due to the stochastic nature of the random vortex method the curves we obtain are a little noisy. We smooth them using a simple 7 point sliding average.

Fig. 3 plots  $\tau$  versus  $x/L$  for different values of  $T$  (these are time averaged values over a period of  $\Delta T = 0.28$ , i.e. the

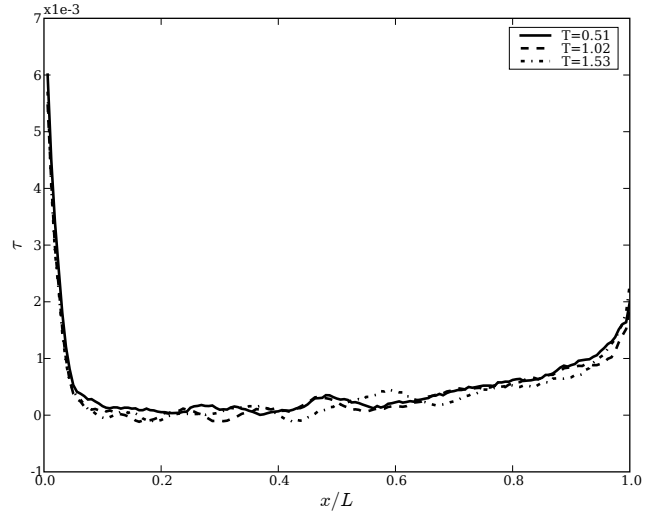


Figure 3. Average  $\tau$  on the outer surface versus  $x/L$  at different times for case 1c.

coupons rotate by about 16 degrees). It is interesting to note that the curves are essentially similar. Fig. 4 plots the variation of  $\tau$  on the outer surface for the cases 1a, 1b, 1c at  $T = 1.53$ . These curves are also time averaged over  $\Delta T = 0.28$  and averaged over all the coupons. It is easy to see that case 1a is not accurate. Thus it is clear that we must choose  $C \leq 11.4$ . Case 1b appears to be a reasonable compromise between cases 1a and 1c.

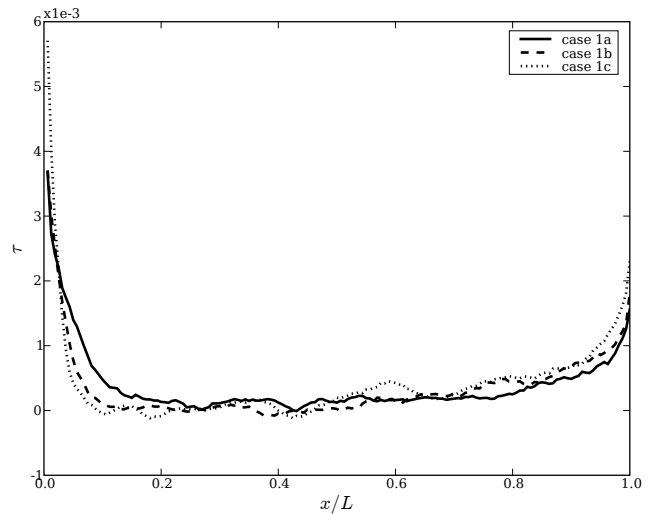


Figure 4. Average  $\tau$  on the outer surface versus  $x/L$  for cases 1a, 1b, and 1c at  $T = 1.53$ .

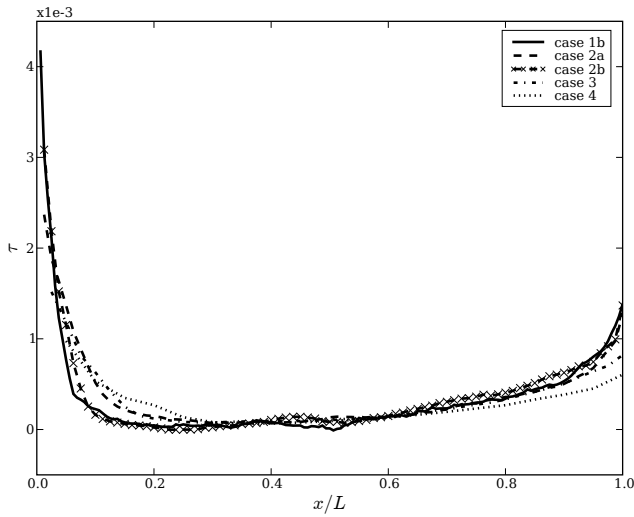


Figure 5. Time averaged  $\tau$  on the outer surface versus  $x/L$  for cases 1a, 2a, 2b, 3 and 4 at  $T = 5.38$ .

Fig. 5 plots the time averaged (over  $\Delta T = 0.57$ ) shear stress on the outer surface at  $T = 5.38$  for various different cases where mainly  $k$  is changing. Clearly, case 4 is not too accurate. Somewhat surprisingly, case 2b is extremely accurate. This suggests that a lower  $C$  value is a good idea if the leading edge stress is to be captured accurately. However the overall stress distribution is reasonable up to about  $k = 0.8$ .

From the results we can see that even though the flow has not reached a steady state, that we get reasonable results up to  $k = 0.4$  but beyond this the results are not as accurate. However, even at larger values of  $k$  we get a good idea about the general variation of the shear stress profile. For the subsequent simulations we attempt to use as small a  $k$  and  $C$  as would be reasonable for the amount of computational time.

### Variation of $Re$

We simulate the rotating cage for various Reynolds numbers. The parameters used are given in Table 2. Clearly, the choice of parameters for the  $Re = 20000$  case could have been better. We will address this in future work. The  $Re = 40000$  simulation takes around 36 hours on a Pentium IV 3 GHz machine.

Figs. 6, 7, 8, and 9 plot the vorticity field and velocity vectors for the flow inside the rotating cage for various Reynolds numbers. Red dots represent vorticity spinning clockwise and blue dots represent anti-clockwise vorticity. It is clear from these that between  $Re = 20000$  and  $Re = 40000$ , there is a change in behavior. It appears that the turbulence in the flow is fully developed at  $Re = 40000$ .

Fig. 10 plots the time averaged shear stress variation ver-

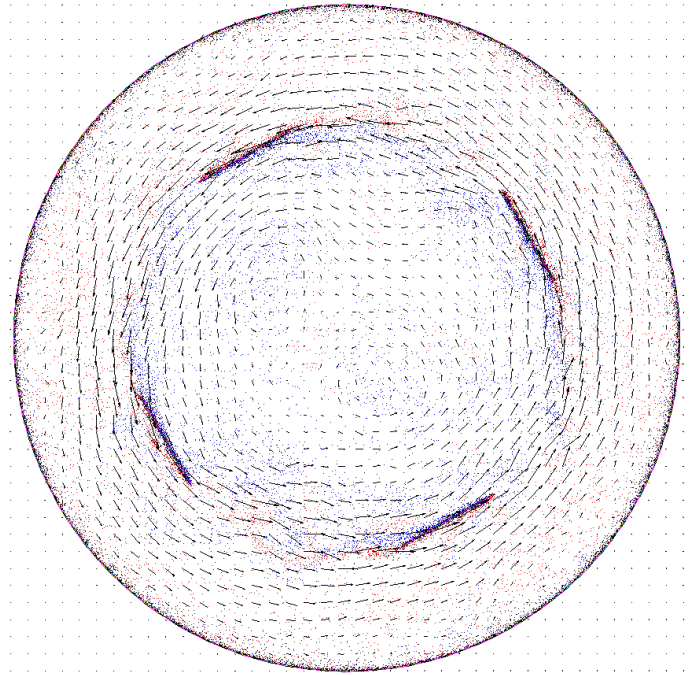


Figure 6. Vorticity and velocity vectors for  $Re = 5000$  at  $T = 11.33$ . Red dots represent vorticity spinning clockwise and blue dots represent anti-clockwise vorticity.

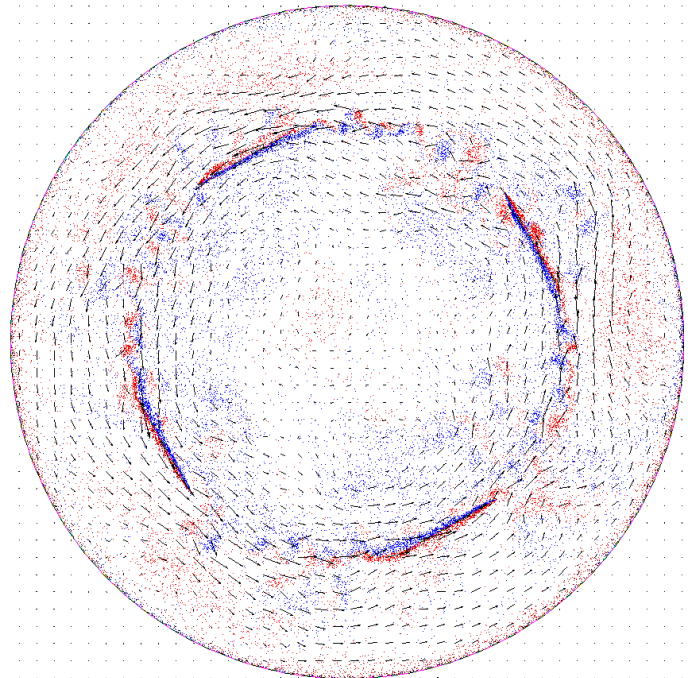


Figure 7. Vorticity and velocity vectors for  $Re = 10000$  at  $T = 11.33$ . Red dots represent vorticity spinning clockwise and blue dots represent anti-clockwise vorticity.

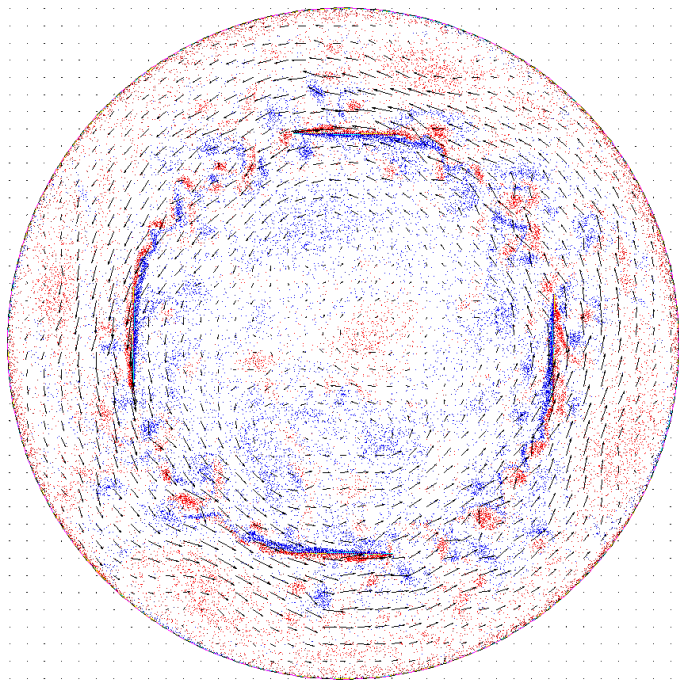


Figure 8. Vorticity and velocity vectors for  $Re = 20000$  at  $T = 17.05$ . Red dots represent vorticity spinning clockwise and blue dots represent anti-clockwise vorticity.

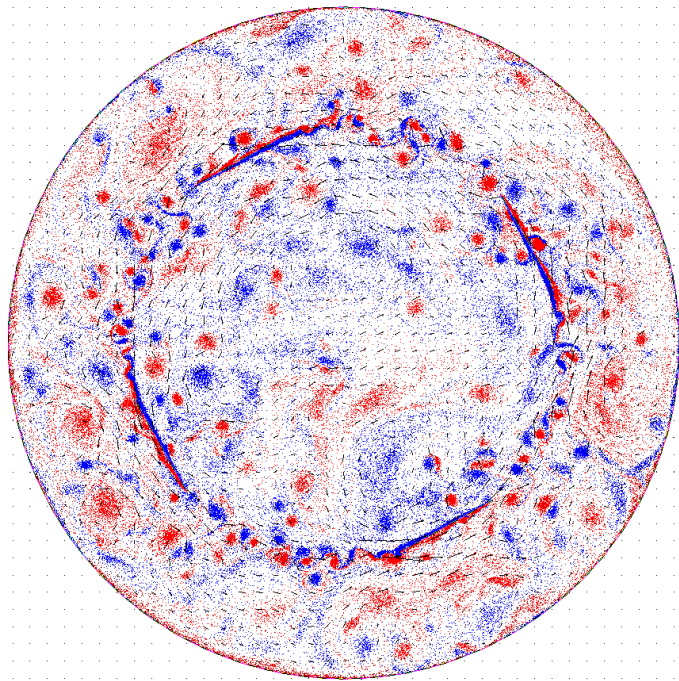


Figure 9. Vorticity and velocity vectors for  $Re = 40000$  at  $T = 11.33$ . Red dots represent vorticity spinning clockwise and blue dots represent anti-clockwise vorticity.

$Re$	$\Omega$	$k$	$C$	$N_{sheet}$	$\gamma_{max}$	$Re_h$
5000	1.78	0.133	8.5	120	0.025	5.85
10000	3.56	0.188	8.5	120	0.025	5.85
20000	7.12	0.4	11.4	80	0.025	8.8
25000	8.9	0.3	5.3	120	0.025	5.85
30000	10.68	0.325	6.4	120	0.025	5.85
35000	12.46	0.351	7.5	120	0.025	5.85
40000	14.24	0.375	8.5	120	0.025	5.85

Table 2. The parameters used for simulation of the rotating cage problem at different Reynolds numbers.  $N_{sheet}$  is the number of sheets released on one side of a coupon.

sus  $x/L$  for various Reynolds numbers on the outer surface of the coupons. As expected the shear stress increases with the Reynolds number. However, there is a significant jump in the shear stress for the Reynolds number of 40000. This along with Fig. 9 clearly suggest the turbulence at this Reynolds number.

Similarly, Fig. 11 plots the time averaged shear stress on the inner surface of the coupon. The behavior of the shear stress in this fashion is understandable since as the flat plate moves, there is a component of the relative velocity that is normal to it near the edges. Thus, the flat plate actually behaves as if it was in a flow with a slight angle of attack.

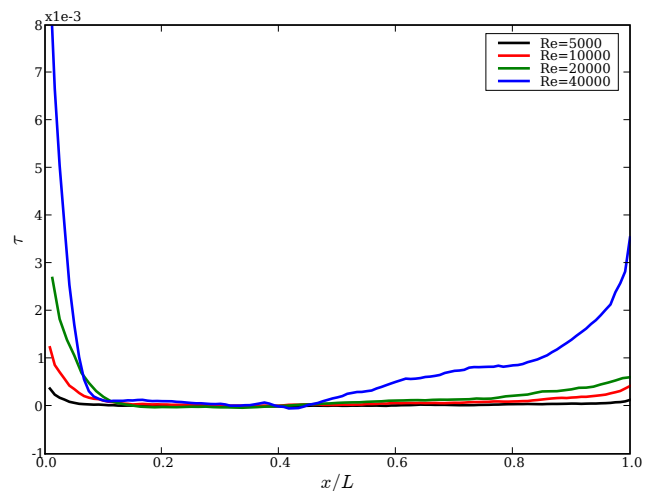


Figure 10. Time averaged  $\tau$  on the outer surface versus  $x/L$  for various Reynolds numbers for  $T > 11$ .

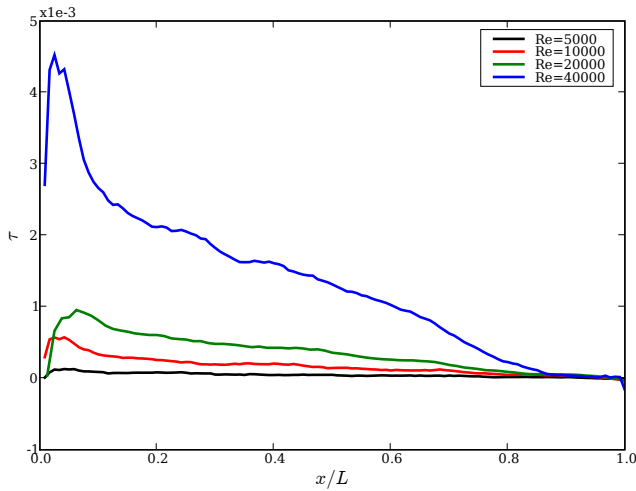


Figure 11. Time averaged  $\tau$  on the lower surface versus  $x/L$  for various Reynolds numbers for  $T > 11$ .

In order to find the Reynolds number around which the shear stress dramatically increases, the time averaged shear stress is plotted in the range  $20000 \leq Re \leq 40000$  in Figs. 12 and 13. The figures suggest that the transition is somewhere between  $Re = 20000$  to  $25000$ .

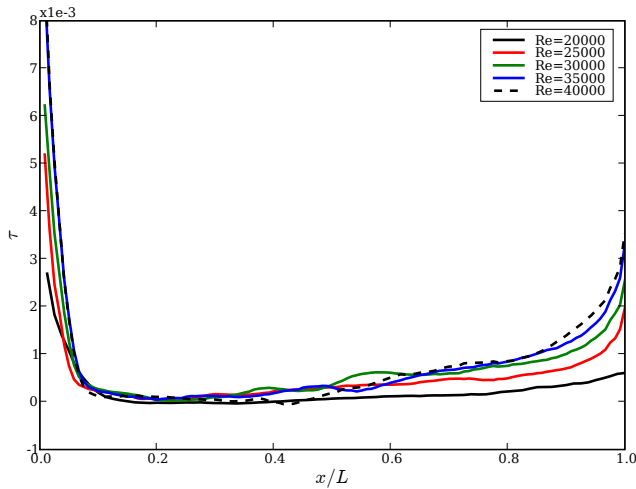


Figure 12. Time averaged  $\tau$  on the outer surface versus  $x/L$  for at  $T > 11$  for Reynolds number in the range  $20000 \leq Re \leq 40000$ .

Fig. 14 plots the average shear stress over all the four coupons, time averaged over a  $\Delta T \approx 0.72$ . Fig. 15 plots the

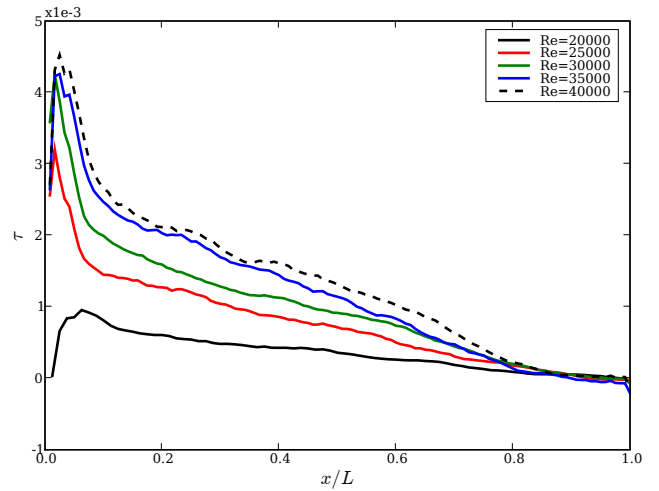


Figure 13. Time averaged  $\tau$  on the lower surface versus  $x/L$  for at  $T > 11$  for Reynolds number in the range  $20000 \leq Re \leq 40000$ .

maximum shear stress averaged over all four coupons and also time averaged over  $\Delta T \approx 0.72$ . It is clear that there is a jump in the shear stress and a change in the slope between  $20000 \leq Re \leq 25000$ . It is also interesting to note that the maximum shear stress is on the upper surface while the average shear stress is higher on the lower surface.

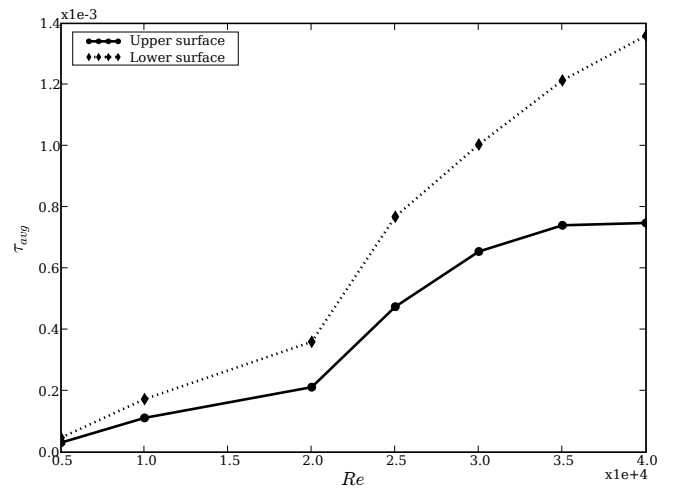


Figure 14. Average  $\tau$  (time averaged) on the coupons versus  $Re$ .

According to the formula given in equation (3) the shear stress for various Reynolds numbers should be as shown in Ta-

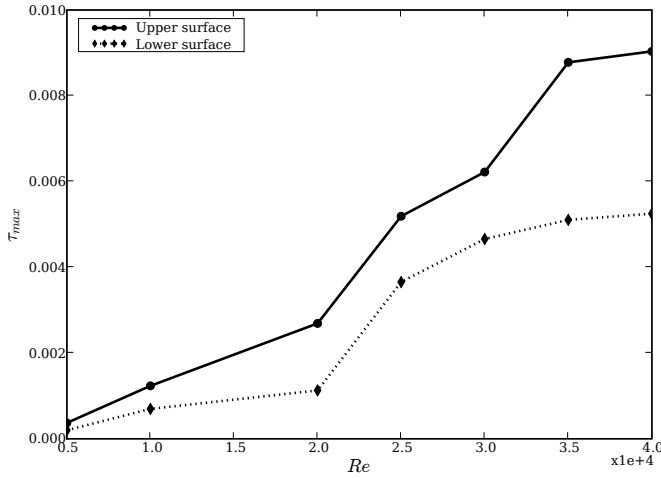


Figure 15. Maximum  $\tau$  (time averaged) on the coupons versus  $Re$ .

ble 3. Approximate estimates for the maximum shear stress on the outer and inner surfaces as computed in this work are also shown. As seen in the various figures, the largest shear occurs near the leading edge of the coupons. The computed shear stress is consistently higher than the one predicted in equation (3). Our simulations indicate that the shear stress distribution is more like that of a flat plate than a circular cylinder in rotation

Table 3. Comparison of shear stresses using equation (3) and computational results. Here we indicate an approximate maximum shear stress that is computed.

$Re$	$\tau$ (from eq. (3))	$\tau_{computed}$ (outer)	$\tau_{computed}$ (inner)
5000	$5.79 \times 10^{-5}$	$2.5 \times 10^{-4}$	$1.3 \times 10^{-4}$
10000	$2.31 \times 10^{-4}$	$1.0 \times 10^{-3}$	$6.0 \times 10^{-4}$
20000	$9.26 \times 10^{-4}$	$2.5 \times 10^{-3}$	$9.0 \times 10^{-4}$
40000	$3.70 \times 10^{-3}$	$8.0 \times 10^{-3}$	$4.5 \times 10^{-3}$

From these results it is clear that the fluid mechanics of this problem is non-trivial. Several important observations can be made.

1. The flow over the coupons is closer to that of a flat plate moving at a slight angle of attack in a fluid than the flow over a rotating cylinder.
2. The shear stress is high on the upper and lower surfaces near the leading edge. These values appear consistently higher than the values predicted by equation (3) as suggested by Schmitt and Bakalli [1]. These results are in good agreement

with the high amount of corrosion observed at the leading edges by [4, 2, 3].

3. The flow at higher Reynolds numbers is highly turbulent. It does not appear as if there is a steady state for the flow.
4. It appears that at some point between  $20000 < Re < 25000$ , the flow transitions into a turbulent regime. This may explain the dramatic increase in the shear stresses when  $Re \geq 25000$ .

The present results are preliminary and cannot be treated as definitive. However, it is clear that these results provide a slightly better understanding of the fluid mechanics of the problem. It is also clear that the existing models are inadequate. There are several interesting questions that remain unanswered.

1. What happens at even higher Reynolds numbers?
2. What is the influence of varying the parameters  $l_c$  and  $l_v$  (i.e. the length of the coupon and the radius of the vessel are changed)?
3. What if the number of coupons is changed?
4. How relevant are these results given the two-dimensionality of the simulations? This can be partially answered by looking at available experimental results.

These and other issues will be addressed in future work.

## CONCLUSIONS

In this work we use a vortex method to simulate the rotating cage problem. The shear stresses on the surface of the coupons are studied in some detail. The results are still preliminary. However, it appears that the flow over the coupons is more like the flow past a flat plate. This explains the high amount of shear near the leading edges. This is in agreement with the conjecture and experimental observations of [4, 2, 3]. The results obtained indicate that the existing empirical formula for the shear stress on the flat plates are conservative estimates.

In the future it would be important to understand the influence of varying  $l_c$ ,  $l_v$  and the number of coupons used. It would be useful to increase the Reynolds number further and study the shear stress. The present work employs a two-dimensional numerical simulation. It is very important to simulate the problem in three dimensions and compare the results.

## ACKNOWLEDGMENT

The author would like to thank Dr. Sunder Ramachandran (Baker Petrolite) for suggesting the problem and for various helpful discussions during the course of this work.

## REFERENCES

- [1] Schmitt, G., and Bakalli, M., 2006. "A critical review of measuring techniques for corrosion rates under flow con-

- ditions". In Proceedings of the 61<sup>st</sup> NACE conference on corrosion, NACE International. Paper number: 06593.
- [2] Ramachandran, S., Ahn, Y. S., Greaves, M., Jovancicevic, V., and Bassett, J., 2006. "Development of high temperature, high pressure corrosion inhibitor". In Proceedings of the 61<sup>st</sup> NACE conference on corrosion, NACE International. Paper number: 06377.
- [3] Ramachandran, S., Mancuso, S., Bartrip, K. A., and Hammonds, P., 2006. "Inhibition of acid gas corrosion in pipelines using glycol for hydrate inhibition". In Proceedings of the 61<sup>st</sup> NACE conference on corrosion, NACE International. Paper number: 06447.
- [4] Dougherty, J. A., Ramachandran, S., and Short, B., 2001. "Does shear stress have an effect on corrosion in sour gas production?". In Proceedings of the 56<sup>th</sup> NACE conference on corrosion, NACE International. Paper number: 01069.
- [5] Chorin, A. J., 1973. "Numerical study of slightly viscous flow". *Journal of Fluid Mechanics*, **57** (4), pp. 785–796.
- [6] Cottet, G.-H., and Koumoutsakos, P., 2000. *Vortex methods: theory and practice*. Cambridge University Press, March.
- [7] Majda, A. J., and Bertozzi, A. L., 2001. *Vorticity and Incompressible Fluid Flow*. Cambridge University Press.
- [8] Ramachandran, P., 2004. *Development and study of a high-resolution two-dimensional random vortex method*. PhD thesis, Department of Aerospace Engineering, IIT-Madras.
- [9] Chorin, A. J., 1978. "Vortex sheet approximation of boundary layers". *Journal of Computational Physics*, **27** (3), pp. 428–442.
- [10] Puckett, E. G., 1991. "Vortex methods: An introduction and survey of selected research topics". In *Incompressible Computational Fluid Dynamics — Trends and Advances*, R. A. Nicolaides and M. D. Gunzburger, Eds. Cambridge University Press, p. 335.
- [11] Puckett, E. G., 1989. "A study of the vortex sheet method and its rate of convergence". *SIAM Journal on Scientific and Statistical Computing*, **10** (2) March, pp. 298–327.
- [12] Shashidhar, S., 1998. Simulation of two dimensional vortex flows. Master's thesis, Department of Aerospace Engineering, IIT-Madras.
- [13] Carrier, J., Greengard, L., and Rokhlin, V., 1988. "A fast adaptive multipole algorithm for particle simulations". *SIAM J. Sci. Stat. Comput.*, **9** (4), pp. 669–686.
- [14] Ramachandran, P., Rajan, S. C., and Ramakrishna, M., 2003. "A fast, two-dimensional panel method". *SIAM Journal on Scientific Computing*, **24** (6), pp. 1864–1878.
- [15] Ramachandran, P., Rajan, S. C., and Ramakrishna, M., 2005. "A fast multipole method for higher order vortex panels in two dimensions". *SIAM Journal on Scientific Computing*, **26** (5), pp. 1620–1642.
- [16] Ramachandran, P., Ramakrishna, M., and Rajan, S. C., To appear. "Efficient rectilinear particle motion in the presence

of complex two-dimensional geometries". *Computers and Mathematics with Applications*.